Behavior of steel-concrete composite cable anchorage system

Article *in* Steel and Composite Structures · January 2018

DOI: 10.12989/scs.2018.26.1.115

CITATIONS
2

READS
109

5 authors, including:

Hongye Gou
Southwest Jiaotong University
22 PUBLICATIONS **34** CITATIONS

SEE PROFILE

Steel and Composite Structures, *Vol. 26, No. 1 (2018) 115-123*
DOI: https://doi.org/10.12989/scs.2018.26.1.115

Behavior of steel-concrete composite cable anchorage system

Hongye Gou[*1,2,3], Wei Wang[3a], Xiaoyu Shi[1b], Qianhui Pu[1c] and Rui Kang[1d]

[1]*Department of Bridge Engineering, School of Civil Engineering, Southwest Jiaotong University, Chengdu 610031, China*
[2]*Key Laboratory of High-Speed Railway Engineering, Ministry of Education, Southwest Jiaotong University, Chengdu 610031, China*
[3]*Department of Civil, Architectural, and Environmental Engineering, Missouri University of Science and Technology, Rolla, MO 65401, USA*

(*Received June 23, 2017, Revised November 26, 2017, Accepted November 30, 2017*)

Abstract. Steel-concrete composite structure is widely applied to bridge engineering due to their outstanding mechanical properties and economic benefit. This paper studied a new type of steel-concrete composite anchorage system for a self-anchored suspension bridge and focused on the mechanical behavior and force transferring mechanism. A model with a scale of 1/2.5 was prepared and tested in ten loading cases in the laboratory, and their detailed stress distributions were measured. Meanwhile, a three-dimensional finite element model was established to understand the stress distributions and validated against the experimental measurement data. From the results of this study, a complicated stress distribution of the steel anchorage box with low stress level was observed. In addition, no damage and cracking was observed at the concrete surrounding this steel box. It can be concluded that the composite effect between the concrete surrounding the steel anchorage box and this steel box can be successfully developed. Consequently, the steel-concrete composite anchorage system illustrated an excellent mechanical response and high reliability.

Keywords: self-anchored suspension bridges; steel-concrete composite cable anchorage system; steel anchorage box; model test; stress distribution; composite effect

1. Introduction

A self-anchored suspension bridge is a suspension bridge in which the main cables are anchored to the stiffening girders of the bridge. It is gradually favored by bridge engineers owing to their artistic appearance, economic benefit, and good adaptability to various topography and geological conditions (Lonetti and Pascuzzo 2014, Qiu *et al.* 2014, 2009, Nie *et al.* 2011). This type of bridge is competitive and frequently used for small and medium spans in urban areas (Xu *et al.* 2017, Lu *et al.* 2014). When comparing with the conventional earth-anchored suspension bridge, no massive anchorages are needed in this type of bridge (Votsis *et al.* 2017, Jung *et al.* 2014, Kim *et al.* 2006). The stiffening girder of a self-anchored suspension bridge carries both the live loads and large horizontal component forces of main cable tension, which makes the main girders become compressive-flexure members (Choi, *et al.* 2014, Gűnaydin *et al.* 2014). Consequently, the mechanical behavior of this type of bridge is more complicated than that of an earth-anchored suspension bridge.

There are four types of cable anchorage systems that are generally applied to self-anchored suspension bridges to transfer the main cable force. The first type is the traditional concrete anchorage system, which is generally large in size. The Guangdong Foshan Pingsheng Grand Bridge that was built in China is a typical application of this anchorage system (Hu *et al.* 2004). The second type is the loop concrete anchorage system, which was applied to the west anchorage of the new San Francisco-Oakland Bay Bridge main suspension span (Sun *et al.* 2004, 2002). However, there are some disadvantages of this system, such as the complicated site construction technology and mechanical behavior of the prestressed concrete anchorage cap beam, the increased strand consumption of the main cable, etc. Then the pure steel anchorage structure is proposed. The Sanchaji Xiang River Grand Bridge in China (Shao *et al.* 2006) and the Yong Jong Grand Bridge in South Korea (Gil and Choi 2001, 2002) are the representative projects that this anchorage system was used. However, there are some concerns that should be concentrated like a large steel consumption, dense stiffeners inside the steel box, resulting in the complicated construction technology, etc. According to the major disadvantages of the three anchorage systems as mentioned above and based on the previous relative studies (Cui *et al.* 2017 a, b, Gou *et al.* 2017 a, b, 2015, Ju and Zeng 2015, Allahyari *et al.* 2014, Papastergiou and Lebet 2014), this paper studied a new type of steel-concrete composite anchorage system and focused on the mechanical behavior and force transferring mechanism. This anchorage system simplifies the structure of pure steel anchorage system, reduces the steel consumption, and improves the

∗Corresponding author, Associate Professor
E-mail: gouhongye@swjtu.cn
[a]Ph.D. Student
E-mail: wwzf3@mst.edu
[b]M.S.
E-mail: shixiaoyuwork@hotmail.com
[c]Professor
E-mail: qhpu@vip.163.com
[d]Associate Professor
E-mail: rkangswjtu@hotmail.com

ISSN: 1229-9367 (Print), 1598-6233 (Online)

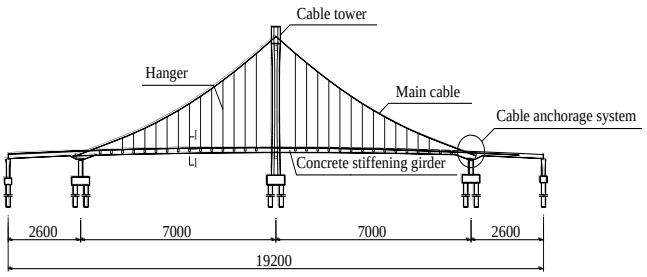

Fig. 1 General profile of Chengdu Qingshui River Bridge (unit: mm)

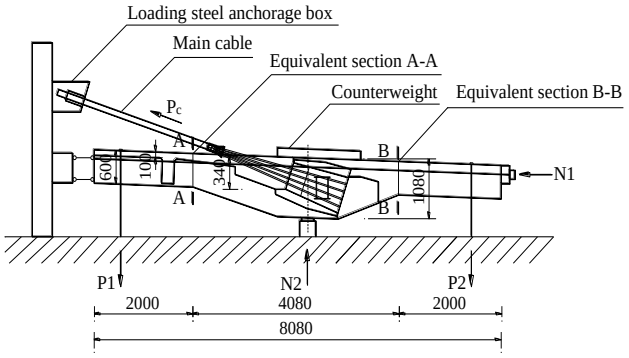

Fig. 2 The overall layout of the test model (unit: mm)

reliability of the weld between steel plates.

There are some studies to examine the mechanical behavior of the cable anchorage systems through model tests and finite element analyses. Shao *et al*. (2006) developed a FEA model and a scaled model to analyze the stress distribution and mechanical behavior of the pure steel anchorage system that was applied to the Sanchaji Xiang River Grand Bridge built in China. Nie *et al*. (2011) carried out a scaled model test and a numerical analysis of the pure steel cable anchorage system for the Qingdao Bay Bridge in China to study the local stress distributions. Su *et al*. (2012) and Lin *et al*. (2015) fabricated model tests of steel-concrete composite cable-pylon anchorage system and evaluated the mechanical behavior of this system. Raftoyiannis and Michaltsos (2016) presented a mathematical model for a damping system as well as its influence on the movable anchorage system. Cheng *et al*. (2013) performed the experimental and FE analyses to investigate the mechanical behavior of the perforated plates in the steel tower anchorage zones of some cable-stayed bridges. However, limited studies are reported on the steel-concrete composite anchorage system for the self-anchored suspension bridge.

The Chengdu Qingshui River Bridge built in China is the first bridge that the steel-concrete composite anchorage system is applied. The bridge has an overall length of 19,200 mm with two main spans of 7,000 mm and side spans of 2,600 mm, as illustrated in Fig. 1. Each main cable consists of 14 strands. Each strand consists of 127 high-strength steel wires that have micro-fine zinc coating, the diameter of each steel wire is 5.3 mm. Each main cable is directly anchored to the prestressed concrete stiffening girder. The main cable in anchorage system is spread by splay saddle. The steel-concrete composite anchorage system is applied to this bridge.

The primary objectives of this study are to enrich the experimental data and investigate the detailed mechanical behavior and force transferred mechanism of the steel-concrete composite anchorage system for the Chengdu Qingshui River Bridge, which is the first bridge that this composite anchorage system is applied in the world. Firstly, a model with a scale of 1/2.5 was prepared and tested in ten loading cases in the laboratory, and their detailed stress distributions were measured. Then, a three-dimensional finite element model was established to understand the stress distributions and validated against the experimental measurement data.

2. Experimental program

2.1 Test model

A model of a main cable anchorage system with the steel-concrete structure of this bridge with a scale of 1/2.5 was fabricated. A half-balancing anchorage system for this scaled model was tested because the horizontal component forces induced by main cable tensions at two anchorage points were equal and opposite. The steel anchorage box was constructed according to design requirements of this new anchorage system to prevent the steel plates from buckling or cracking when applying the load to the experimental model. The horizontal and transverse boundary conditions of this model were simulated by using the roller restraints. The main cable was installed to a reaction wall. One side of this test model was anchored to another reaction wall. Fig. 2 illustrates the overall layout of the model of this test.

The overall length of this model was 8,080 mm. The beam height of variable section was linearly varied from 600 mm to 1080 mm as shown in Fig. 2. The width was 3,000 cm. The thickness of the lateral flange plate of the stiffening girder varied linearly from 100 mm to 340 mm. The axial load was applied by a jack. The shear force and moment can be induced by the ground anchors. The outside of the anchorage system was attached the steel and polyethylene plates. The compressive force induced by installation of the prestressed tendons applied to the polyethylene plate, which simulates the roller restraints.

2.2 Material properties

The materials used in this study were consistent with those of the actual bridge to guarantee that the test model has a similar mechanical response to that of the actual anchorage structure.

According to the AISC code (2010), concrete should have a compressive strength, $f_c^{'}$, of not less than 21.00 MPa nor more than 70.00 MPa. The stiffening girder was cast using a concrete with a 28 day compressive strength of 50.30 MPa. The final modulus of elasticity of concrete E_c was 3.28×10^4 MPa, tensile strength f_t was 2.25 MPa.

The steel anchorage box consists of the rear anchorage plate, inner web plate, front anchorage plate, top anchorage

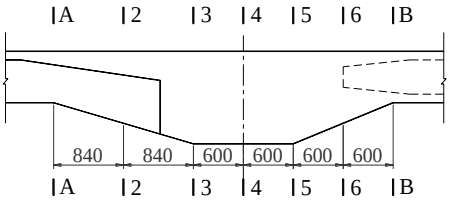

Fig. 3 The test sections of the concrete in anchorage system (unit: mm)

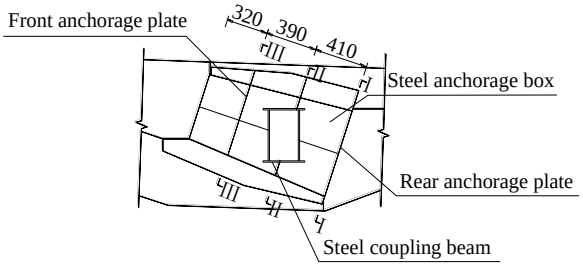

Fig. 4 The test sections of steel anchorage box (unit: mm)

plate, shear plate, and other lateral plates. The steel grade of the steel anchorage structure was Q345C. The yield and ultimate strength of the steel plates specified by the manufactures were respectively 310.00 MPa and 470.00 MPa. The strength of the steel plates meets the requirement of material grade. Furthermore, the φ15.2 prestressed tendons were used in this study. The characteristic value of the tensile strength is 1,860.00 MPa.

2.3 Loading scheme

According to the equivalence of stress, the equivalence sections of the experimental model were selected in sections A-A through B-B, as illustrated in Fig. 2. The equivalence force was determined, then the self-weight of concrete was considered to determine the horizontal and transverse equivalent force that should be applied to the specimen. A jack of 500 t and prestessed cables consisted of the loading system of the experimental model. These cables were tensioned by the jack, which loads the experimental model to simulate the main cable force. To simulate the equivalent load at the section B-B, the end of the specimen was applied the axial load (N1). The distance was 1,500 mm between the section B-B and this end. Two steel strands connected with the model were anchored to the floor of the laboratory to form lateral ground anchor forces (P1 and P2). The reaction of the anchorage location was N2. The details are illustrated in Fig. 2. Because the shear force of this experimental model had a little influence on the test results, it was not considered in this study. The moment of this model was determined based on the equivalence stress.

According to the inter force calculation of construction process for the Chengdu Qingshui River Bridge, there were a total 43 construction procedures. Because the ground anchor force was formed by the steel strands tensioned, it was easy to increase. The force, however, was difficult to decrease after the force was increased. According to the variation of this anchor force, the load conditions of this experimental model were adjusted after the system transformation. Finally, the model test was divided 10 load conditions in this study. Table 1 demonstrates the load conditions after adjustment.

The loading procedures and levels, the main cable forces, the ground anchor forces, and the reactions before and after the system transformation were illustrated in Table 2, respectively. For load conditions 1, 2, 4, 5, 6, 7, and 8, the load was applied at four levels. The first level was 0.4 time the design maximum main cable force; the second level was 0.6 time the design maximum main cable force; the third level was 0.8 time the design cable force; and the last one was the design maximum cable force. For load conditions 3, 9, and 10, the applied load was the design maximum main cable force. To perform this loading test, 4 jacks, 8 steel strands, 8 resistance transducers, and 3 hydraulic capsules were used.

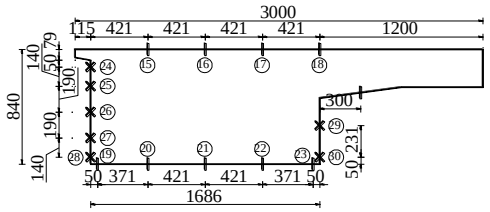

(a) Section 2-2

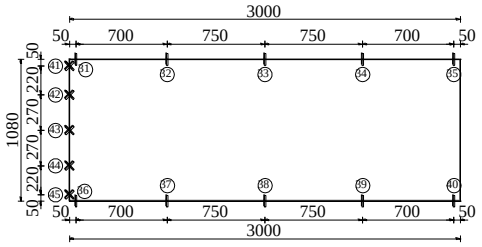

(b) Sections 3-3 through 5-5

Fig. 5 Arrangement of the strain measuring device on the concrete in anchorage system (unit: mm)

2.4 Test setup and procedure

The stress distributions of the anchorage system were complicated. In addition, variable sections of the stiffening girder and composite joint between the steel anchorage box and this girder were also complex. Therefore, equivalent Sections A-A and B-B and Sections 2 through 6 at the anchorage system of the concrete stiffening girder were tested, as shown in Fig. 3.

As illustrated in Fig. 4, Section I-I is the location of the rear anchorage plate. The joint between the steel coupling beam and the steel anchorage box is considered Section II-II. The location of the front anchorage plate is regarded as Sections III-III.

2.5 Arrangement of strain measuring device

2.5.1 Concrete in anchorage system

The strain gauges were arranged at the locations of these 7 sections to measure the concrete strains. In addition, the strain rosettes were arranged at the end of the girder and along the direction of the normal compressive and the

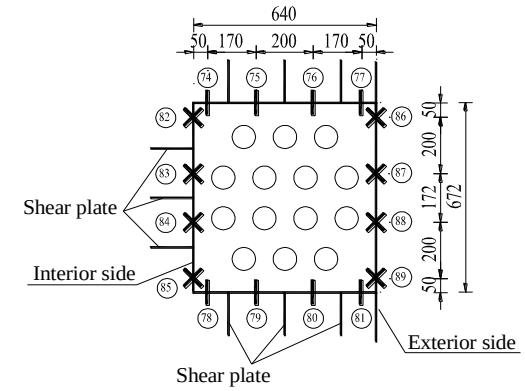

(a) Section I-I

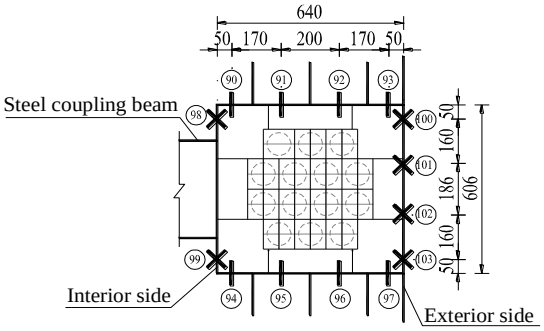

(b) Sections II-II

Fig. 6 Arrangement of the strain measuring devices on the steel anchorage box (unit: mm)

tensile stresses located at the 7-section areas of the girder to measure the concrete strains owing to the complex mechanical behavior of these areas. Fig. 5 illustrates the arrangement of the strain gauges for partial concrete test section in the anchor zone.

2.5.2 Steel anchorage box

The measuring points of the steel strain measuring devices are numbered as shown in Fig. 6. The steel strain gauges were attached to the locations of Sections I through IV of the steel anchorage box. Due to the complicated stress distribution on the steel anchorage box, to attain the stress state of this box, several 45° 3-axis strain rosettes were arranged at the steel plates. These measuring devices were coated by epoxy resin to protect them from the concrete during casting.

3. Finite-element model

An elaborate FEA of this experimental model was performed by using the commercial FE package ANSYS. According to the experimental results, the FE approach and its assumptions were completely confirmed. The experimental results were effectively supplemented by the FEA results. Fig. 7 exhibits the elaborate 3D geometry model of the test model.

Nodes and elements were produced by using the free meshing of the geometry model. Shell elements SHELL63 and solid elements SOLID45 are used to simulate the steel plates of steel anchorage box and the concrete, respectively. The total elements were 112,740 including 7,110 shell elements and 105,630 solid elements. There were 31,123 nodes in this numerical model.

When analyzing the experimental model, the vertical and horizontal displacements were constrained by the end of the stiffening girder. A complete composite effect between the steel and concrete was considered. In addition, the slip effect between the steel and concrete was ignored. The equivalent concentrated force was applied to the model.

4. Results and discussions

For load conditions 1 through 3, the experimental model with full scaffold was applied load because these conditions were performed before the system transformation. The test model without scaffold was applied force because the load cases 4 through 10 were constructed after the system transformation. The normal stress distribution at the front and rear anchorage plates of the steel anchorage box, the joint area between the steel anchorage box and steel coupling beam, and the concrete in anchorage system were analyzed under the load conditions 4 through 10 in this paper.

4.1 Stress of the front anchorage plate

No crack and buckling of this experimental anchorage system was observed in the model test. The maximum tensile strength of 50.95 MPa was measured at the exterior side of the front anchorage plate under the load condition 6. This anchorage box was considered safe and reliable due to very low stress level of each location of the front anchorage

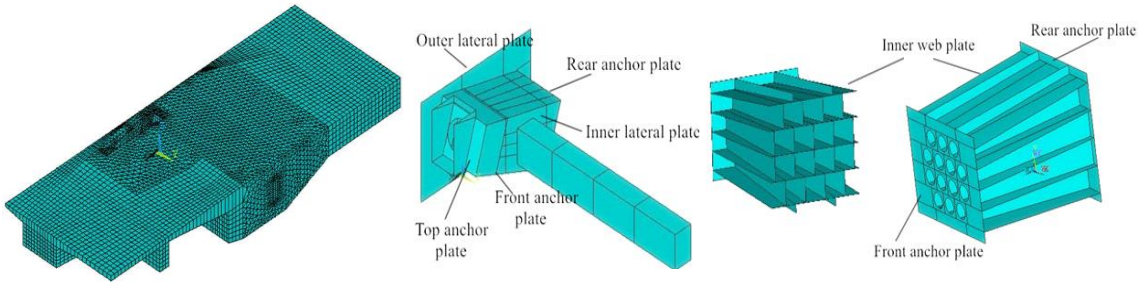

(a) General view of anchorage zone (b) Steel coupling beam and steel anchorage box

Fig. 7 Geometry model of main cable anchorage system established by using ANSYS

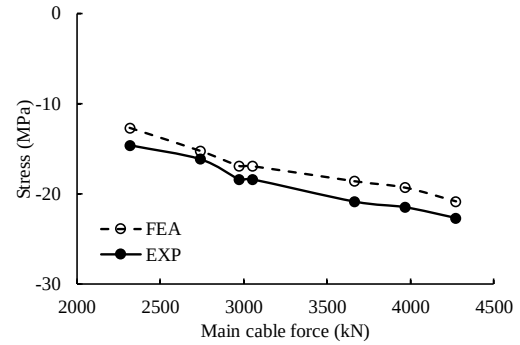

(a) Top surface

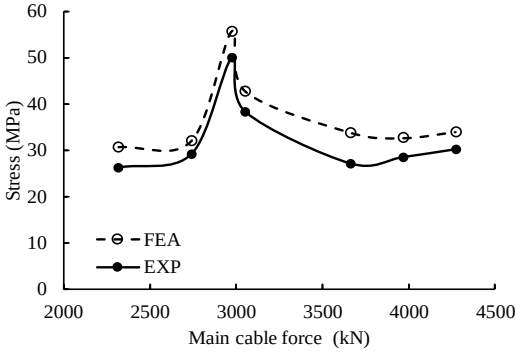

(b) Exterior side

Fig. 8 Experimental and FEA results of average normal stresses of the front anchorage plate

plate under each load condition, which indicates reasonability of the design.

The small observed differences between the experimental and numerical results demonstrate that the design and assumption of FEA model are reasonable. No damage is observed at the joint area between the steel anchorage box and the concrete, which indicates that the composite effect can be developed between this steel box and the stiffening girder. In addition, it can be verified that the concrete surrounding the steel anchorage box is under compressive condition owing to the influence of the steel bars located at holes of PBL member. Thus, the concrete surrounding this anchorage box has a similar condition with the hoop effect of concrete-filled steel tubular member, which shows the effectiveness of PBL shear connectors.

The top and bottom surface and the interior surface of the front anchorage plate are under the compression. The linear relationship between the normal stress and main cable force are observed in Fig. 8 (a). However, it should be noted in Fig. 8 (b) that the relationship is not linear. The reason may be that the reflection point of this curve was occurred under the load condition 6 (see Table 1), the tensile stress of the exterior side of this plate had a significant increase.

4.2 Stress of the rear anchorage plate

The maximum experimental compressive and tensile stresses of 31.66 MPa and 46.45 MPa were measured at the interior and exterior side of the rear anchorage plate under the load condition 10, respectively. The almost linear relationship is observed in Fig. 9 (a). The FEA results correlate well with the experimental measurements, which shows that the establishment and assumption of FEA model are reasonable. Because very low stress level of each location of the rear anchorage plate under every load condition is observed, the steel anchorage box is considered safe and reliable.

It should be noted in Fig. 9 (b) that the relationship between the normal stress and main cable force is not linear. The possible explanation is that the inflection point of this curve was occurred when the load condition had an adjustment.

4.3 Stress of the joint area between steel anchorage box and steel coupling beam

Table 1 The description of the load conditions after adjustment

Load condition for the model test	Load condition for actual bridge	Description of load condition
Before system transformation		
1	1	Prestressed tendons were tensioned
2	2	The experimental model was applied force after the main cable was installed
3	3	The experimental model was applied force after the hangers were installed
After system transformation		
4	4	The hangers were tensioned and the system was transforming
5	7	The experimental model was applied the design maximum cable force
6	6	The hangers were tensioned for the third time
7	5	The hangers were tensioned for the second time
8	8	The model was tensioned by 1.2 times design maximum main cable force
9	9	The model was tensioned by 1.3 times design maximum main cable force
10	10	The model was tensioned by 1.4 times design maximum main cable force

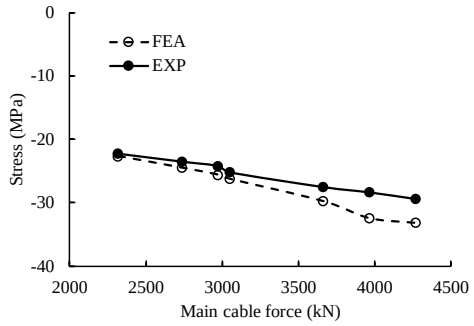

(a) Top surface

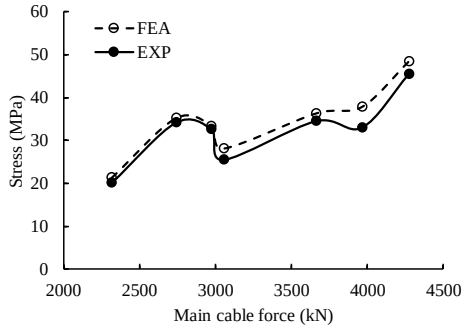

(b) Exterior side

Fig. 9 Experimental and FEA results of average normal stresses of the rear anchorage plate

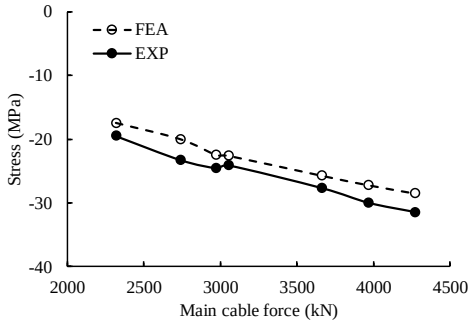

(a) Bottom surface

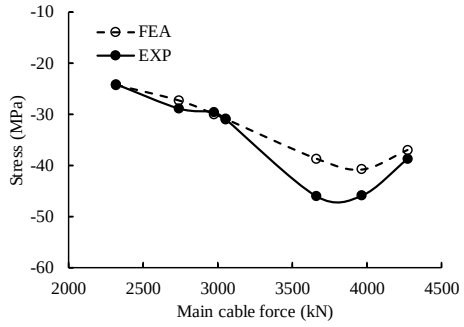

(b) Exterior side

Fig. 10 Experimental and FEA results of average normal stresses of the joint area

The maximum compressive strength of 47.10 MPa was measured at the exterior side of Section II-II under the load condition 8. The almost linear relationship is observed in Fig. 10 (a). It should be noted in Fig. 10 (b) that the relationship between the normal stress and main cable force

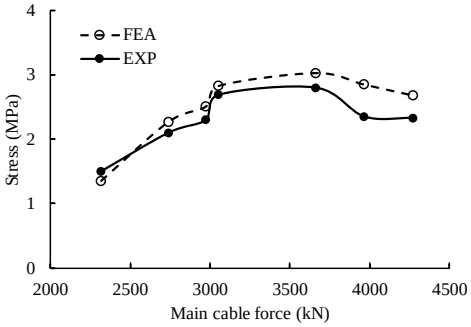

(a) Top surface of Section 6-6

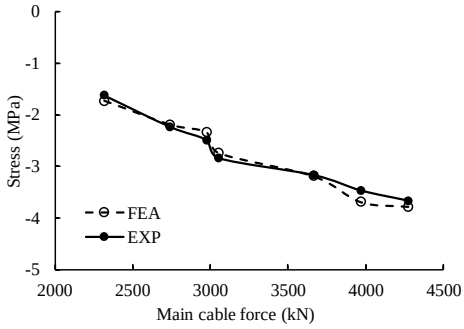

(b) Bottom surface of Section 6-6

Fig. 11 Experimental and FEA results of average normal stresses of the concrete in anchorage system

is not linear. The possible explanation is that the reflection point in this curve was occurred under the load condition 8 (see Table 1), the compressive and tensile stresses of the exterior side of the joint area had a remarkable decrease with the increase of the main cable force.

No damage and crack was observed at the joint, which exhibits the excellent composite effect between the steel anchorage box and the concrete. The steel anchorage box and the steel coupling beam are considered safe and reliable.

4.4 Stress of the concrete stiffening girder in anchorage system

The normal stress of the top surface changes from compressive stress to tensile stress for each test section, and the compressive stress of the bottom surface gradually increases with the increase of the main cable force. Sections 2-2 and 3-3 are under the compressive condition. No damage and cracking is observed at the concrete surrounding the steel anchorage box. The top surfaces of Sections 5-5, 6-6, and B-B show high stress levels. As shown in Fig. 11, the maximum tensile stress of 3.05 MPa was measured at the top surface of Section 6-6 under the load condition 8. A tiny crack was first observed on the top surface of the flange of Section B-B, with the maximum tensile stress of 2.39 MPa which exceed the tensile strength of concrete. It may be caused by the shear-lag effect of the stiffening girder section. In addition, the equivalent boundary condition of the test model had an influence on the high stress levels.

Due to the load condition 5 corresponding to the system

Table 2 The loading levels and applied forces (unit: kN)

Load condition	Loading level	Main cable force	Ground anchor force P1	Ground anchor force P2	The axial force N1	The reaction N2
1	0.4	0	80	72	920	N/A
	0.6	0	120	108	1380	
	0.8	0	160	144	1840	
	1.0	0	200	180	2300	1372
2	0.4	44	200	180	2300	N/A
	0.6	65	200	180	2300	
	0.8	87	200	180	2300	
	1.0	109	210	180	2300	1338
3	1.0	125	210	180	2300	1332
4	0.4	927	72	48	2300	N/A
	0.6	1390	108	72	2300	
	0.8	1854	144	96	2300	
	1.0	2317	180	120	2300	492
5	0.4	2611	180	120	2300	N/A
	0.6	2759	190	120	2300	
	0.8	2906	190	120	2300	
	1.0	3053	200	120	2300	306
6	0.4	3021	216	140	2300	N/A
	0.6	3006	224	150	2300	
	0.8	2990	232	160	2300	
	1.0	2974	241	170	2300	509
7	0.4	2960	262	198	2300	N/A
	0.6	2953	273	212	2300	
	0.8	2946	284	226	2300	
	1.0	2739	295	240	2300	827
8	0.4	3109	295	240	2300	N/A
	0.6	3293	295	240	2300	
	0.8	3478	295	240	2300	
	1.0	3663	295	240	2300	
9	1.0	3967	295	240	2300	N/A
10	1.0	4273	295	240	2300	N/A

transformation of the actual construction stage of this bridge, design and reinforcement of the stiffening girder at Sections 5-5, 6-6, and B-B may be adjusted because high tensile stress levels are illustrated at these sections. At the same time, the special concern should be focused on the concrete located at the rear anchorage plate because the large tensile strength is observed at the location.

4.5 Stress distribution

Fig. 12 exhibits the stress distribution of the concrete stiffening girder in anchorage system. It can be concluded that the compressive stress of the concrete from Section A-A to Section B-B is increasing and then decreasing gradually. In contrast, the tensile stress of the concrete from Section A-A to Section B-B is increasing gradually.

More specifically, Section 3-3 exhibits the maximum compressive stress value of 23.30 MPa among these sections that is much less than the compressive strength of concrete (50.30 MPa). However, the high local tensile

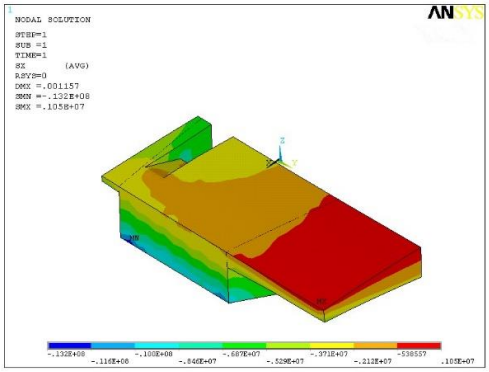

(a) Section A-A

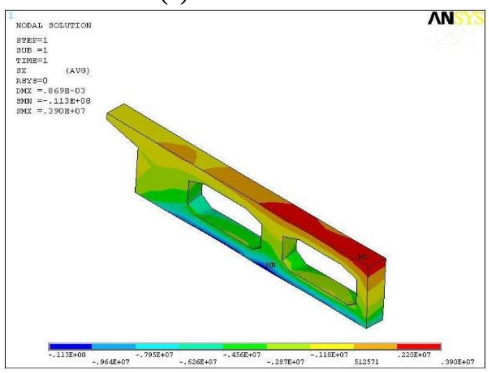

(b) Section B-B

Fig. 12 Stress nephograms of the concrete in anchorage system under load condition 10

stresses of Sections B-B were 3.90 MPa, which exceed the tensile strength of concrete. Thus, to effectively reduce the cracking of the concrete and sufficiently develop the composite effect of the steel-concrete composite anchorage system, the distribution bars should be designed at the tension zone of concrete. In addition, the procedure of the cable adjustment needs to be detailed to reduce the unfavorable moment under the load condition 5.

5. Conclusions

Based on the above investigations, conclusions can be drawn as follows:

- Even if the complex stress distribution at the steel anchorage box is observed in this model test, the stress distribution at each steel plate is relatively uniform due to the constraint effects of the concrete inside this anchorage box. The experimental results generally correlate with the FEA results. The overall stress level of the steel anchorage box is low, which indicates the design of the steel anchorage box is safe and reliable.
- Located at the top surface of each section, the concrete in the anchorage system is under the tensile condition. In contrast, the compressive stress is carried by the bottom of the concrete for each section. No damage and cracking is observed at the concrete surrounding the steel anchorage box. It can be concluded that the composite effect between the concrete surrounding the steel anchorage box and this steel box can be

successfully developed. A tiny crack on the top surface of the flange of Section B-B is firstly observed under the load condition 5. It is necessary that proper construction techniques should be adopted to prevent concrete from cracking in actual construction of this bridge.

• The main cable force is transferred by anchorage device to the rear anchorage plate, then it is transferred by the rear anchorage plate to the lateral plates of the steel anchorage box and the inner vertical and horizontal webs, and to the front anchorage plate and the lateral plates that connects with the concrete of the stiffening girder. Next, the main cable force is transferred by the shear members that connects the steel anchorage box with the concrete to the concrete stiffening girder. Consequently, the steel-concrete composite cable anchorage system exhibits an excellent mechanical behavior with high reliability.

• The experimental and numerical results can effectively demonstrate the stress distribution and force transferring mechanism of the steel-concrete composite anchorage system, which indicates the design of this anchorage system is reliable and safe. This study, therefore, can be considered a reference of steel-concrete composite anchorage system to design the self-anchored suspension bridges.

Acknowledgments

The research described in this paper was financially supported by the National Natural Science Foundation of China (Grant No. 51108382), the Fundamental Research Funds for the Central Universities (Grant No. 2682015CX07), and the Science and Technology Research and Development Plan of China Railway Construction (Grant No. 2014-C34). The visiting scholarship for the first author to visit the Department of Civil, Architectural and Environmental Engineering at the Missouri University of Science and Technology (Rolla, MO) was made possible by the Chinese Scholarship Council (Grant No. P-1-02556).

References

AISC (2010), Load and resistance factor design (LRFD) specification for structural steel buildings, Chicago, IL.

Allahyari, H., Dehestani, M., Beygi, M.H., Neya, B.N. and Rahmani, E. (2014), "Mechanical behavior of steel-concrete composite decks with perfobond shear connectors", *Steel Compos. Struct.*, **17**(3), 339-358.

Cheng, B., Wang, J.L. and Li, C. (2013), "Compression behaviour of perforated plates in steel tower anchorage zones of cable-stayed bridge", *J. Constr Steel Res.*, **90**, 72-84.

Choi, D.H., Gwon, S.G. and Na, H.S. (2014), "Simplified analysis for preliminary design of towers in suspension bridges", *J. Bridge Eng.*, **19**(3), 04013007.

Cui, K., Yang, W.H. and Gou, H.Y., (2017a), "Experimental research and finite element analysis on the dynamic characteristics of concrete steel bridges with multi-cracks", *J. Vibroeng.*, **19**, 4198-4209.

Cui, K., Zhao, T.T. and Gou, H.Y. (2017b), "Numerical study on parameter impact on fundamental frequencies and dynamic characteristics of pre-stressed concrete beams", *J. Vibroeng.*, **19**, 1680-1696.

Gil, H. and Choi, Y. (2001), "Cable erection test at pylon saddle for spatial suspension bridge", *J. Bridge Eng.*, **6**(3), 183-188.

Gil, H. and Choi, Y. (2002), "Cable erection test at splay band for spatial suspension bridge", *J. Bridge Eng.*, **7**(5), 300-307.

Gou, H.Y., Long, H., Bao, Y., Chen, G.D., Pu, Q.H. and Kang, R. (2017a), "Experimental and numericalstudies on stress distributions in girder-arch-pier connections of long-span continuous rigid frame arch railway bridge", *J. Bridge Eng.* (accepted)

Gou, H.Y., Pu, Q.H., Zhou, Y. and Hong, Y. (2015), "Arch-to-beam rigidity analysis for V-shaped rigid frame composite arch bridges", *Steel Compos. Struct.*, **19**(2), 405-416.

Gou, H.Y., Shi, X.Y., Zhou, W., Cui, K. and Pu, Q.H. (2017b), "Dynamic performance of continuous railway bridges: Numerical analyses and field tests", *Proc. IMechE. Part F: J. Rail Rap. Tran.*, DOI: 10.1177/0954409717702019.

Gűnaydin, M., Adanur, S. Altunişik, A.C., Sevım, B. and Tűrker, E. (2014), "Determination of structural behavior of Bosporus suspension bridge considering construction stages and different soil conditions", *Steel Compos. Struct.*, **17**(4), 405-429.

Hu, J.H., Xiang, J.J. and Liao, J.H. (2004), "Conceptual design of a single-tower self-anchored suspension bridge: Scheme design of Foshan Pingsheng Bridge", *Proceedings of the 16th National Bridge Academic Conference*, Beijing, China.

Ju, X.C. and Zeng, Z.B. (2015), "Study on uplift performance of stud connector in steel-concrete composite structures", *Steel Compos. Struct.*, **18**(5), 1279-1290.

Jung, M.R., Shin, S.U., Attard, M.M. and Kim, M.Y. (2014), "Deflection theory for self-anchored suspension bridges under live load", *J. Bridge Eng.*, **20**(7), 1-19.

Kim, H.K., Leeb, M.J. and Chang, S.P. (2006), "Determination of hanger installation procedure for a self-anchored suspension bridge", *Eng. Struct.*, **28**, 959-976.

Lin, Z.F., Liu, Y.Q. and He, J. (2015), "Static behaviour of lying multi-stud connectors in cable-pylon anchorage zone", *Steel Compos. Struct.*, **18**(6), 1369-1389.

Lonetti, P. and Pascuzzo, A. (2014), "Design analysis of the optimum configuration of self-anchored cable-stayed suspension bridges", *Struct. Eng. Mech.*, **51**(5), 1-20.

Lu, P., Chen, J., Zhong, J. and Lu, P. (2014), "Optimization analysis model of self-anchored suspension bridge", *Math. Prob. Eng.*, **2014**, 1-8.

Nie, J.G., Tao, M.X. and Fan, J.S. (2011), "Research on cable anchorage systems for self-anchored suspension bridges with steel box girders", *J. Bridge Eng.*, **16**(5), 633-643.

Papastergiou, D. and Lebet, J.P. (2014), "Investigation of a new steel-concrete connection for composite bridges", *Steel Compos. Struct.*, **17**(5), 573-599.

Qiu, W., Jiang, M. and Zhang, Z. (2009), "Research on limit span of self-anchored suspension bridge", *Comput. Struct. Eng.*, 1173-1180.

Qiu, W.L., Jiang, M. and Zhang, Z. (2014), "Responses of self-anchored suspension bridge to sudden breakage of hangers", *Struct. Eng. Mech.*, **50**(2), 241-255.

Raftoyiannis, I.G. and Michaltsos, G.T. (2016), "Movable anchorage systems for vibration control of stay-cables in bridges", *Eng. Struct.*, **112**, 162-171.

Shao, X.D., Deng, J., Li, L.F. and Jiang, Z.X. (2006), "Cable anchorage structure of self-anchored suspension bridge", *China Civil Eng. J.*, **39**(7), 81-87. (in Chinese)

Su, Q.T., Yang, G.T., Qin, F. and Wu, C. (2012), "Investigation on the horizontal mechanical behaviour of steel-concrete composite cable-pylon anchorage", *J. Constr. Steel Res.*, **72**, 267-275.

Sun, J., Manzanarez, R. and Nader, M. (2002), "Design of looping cable anchorage system for new San Francisco-Oakland Bay

Bridge main suspension span", *J. Bridge Eng.*, **7**(6), 315-324.
Sun, J., Manzanarez, R. and Nader, M. (2004), "Suspension cable design of the new San Francisco-Oakland Bay Bridge", *J. Bridge Eng.*, **9**(1), 101-106.
Votsis, R.A., Stratford, T.J., Chryssanthopoulos, M.K. and Tantele, E.A. (2017), "Dynamic assessment of a FRP suspension footbridge through field testing and finite element modelling", *Steel Compos. Struct.*, **23**(2), 205-215.
Xu, F.Y., Zhang, M.J., Wang, L. andZhang Z. (2017), "Self-anchored suspension bridges in China", *Pract. Period. Struct. Des. Constr.*, **22**(1), 04016018.

CC